

Optimizing solar cells: a comparative study of delafossite HTLs with CsPbI₃ and CsSnI₃ for enhanced stability and efficiency

Al. A. Siddique ^a, M. S. Rasel ^a, M. I. Haque ^{b,*}, S. Bin. Helal ^b, S. A. Saimon ^b, S. Hannan ^c, M. H. Bhuyan ^d, L. C. Paul ^e

^a *Department of Electrical and Electronic Engineering, East Delta University, Chattogram, Bangladesh*

^b *Department of Electrical and Electronic Engineering, International Islamic University Chittagong, Chattogram, Bangladesh*

^c *Department of Electrical and Telecommunication Engineering, International Islamic University Chittagong, Chattogram, Bangladesh*

^d *American International University – Bangladesh*

^e *Department of Electrical Electronics and computer Engineering, Pabna University of Science and Technology*

This research replaces conventional hole transport layers (HTLs) like Spiro-OMeTAD, with Cu-based delafossite materials for improved performance. CsSnI₃ and CsPbI₃ were used as absorber layers to enhance perovskite solar cells (PSCs) stability. Various PSCs were optimized by adjusting perovskite thickness, HTL thickness, and temperature to determine their influence on efficiency. The results were examined to determine the highest-performing PSC, offering insights into stable and cost-effective solar cell designs for better energy harvesting.

(Received February 17, 2025; Accepted May 29, 2025)

Keywords: Perovskite solar cell, Delafossite based solar cell, High performance, High efficiency, Stability

1. Introduction

These days, we depend a lot on fossil fuels, and burning them ranks as a major factor in global warming [1]. The main reasons for the energy crisis of many developing nations are the reliance on coal, oil, and natural gas for energy and the unstable energy market [2]. So, it is time to look for a new, reliable, and secure substitution for fossil fuels. Renewable energies like solar, biogas, wind energy, wave energy, hydropower, and geothermal energies can be great substitutions for fossil fuels and save our world [3–10]. Solar energy is quickly becoming the frontrunner among renewable energy options, thanks to its limitless supply and promise to tackle the global energy shortage. In 2022, it stood out as the second most widely adopted renewable energy system across the globe with a capacity of 1056 GW, and currently, solar cells are contributing 3.6% of global energy production [11]. Researchers have designed many kinds of solar cells during the last two decades and among all those solar cells, perovskite has drawn the most attention. Perovskite is a material which has a chemical structure of MNR₃ where M is an organic positively charged ion, N is a metallic positively charged ion, and R is a negatively charged halogen ion [12]. Perovskite materials have garnered substantial focus within the scholarly fraternity owing to their superior electrical and optoelectronic performance metrics. These materials exhibit ambipolar charge transport capabilities with high carrier mobilities, exceptionally low exciton binding energies facilitating efficient charge separation, and extended carrier diffusion lengths conducive to effective charge collection. Furthermore, perovskites demonstrate a high optical absorption coefficient across a broad spectral range, minimal trap state densities that mitigate non-radiative recombination losses,

* Corresponding author: ismail07rueteeee@iiuc.ac.bd
<https://doi.org/10.15251/JOR.2025.213.319>

and an intrinsically tunable bandgap, enabling spectral optimization for a variety of photovoltaic and optoelectronic applications [12–17]. Even though researchers favor PSC, it still has many disadvantages and one of the main disadvantages of PSC is its organic cation [18,19]. There are mainly two types of organic cations that are used in PSCs namely MA^+ (methylammonium), and FA^+ (formamidinium). MA^+ is unstable under thermal and light illumination conditions which mainly result from the high volatility of the hydrophobic nature of MA^+ cation under such external stimuli [20,21]. Methylammonium (MA^+)-based PSCs experience a phase shift from a tetragonal to cubic structure at 55°C , which is close to the operational temperature of these devices [22]. This transition can negatively affect the photo and heat resistance of the cells. Additionally, MA^+ based perovskites are known to degrade under heat and light exposure due to their low crystallization energy [23–25], and the volatile nature of MA^+ makes it unsuitable for large-scale production. Recently, formamidinium (FA^+) has emerged as a preferred alternative to MA^+ , offering advantages such as a narrower bandgap for enhanced light absorption, longer charge diffusion lengths, and better photostability [26–33]. FA^+ based perovskites can crystallize into two distinct structural phases depending on the thermal conditions applied: a yellow hexagonal non-perovskite phase or a black trigonal perovskite phase. Significantly, FAPbI_3 maintains structural stability within the temperature range of 25°C to 150°C , exhibiting no phase transitions throughout this interval [22,30]. Nevertheless, the presence of various defects in FA^+ -based perovskites—including intrinsic point defects, grain boundary irregularities, and surface imperfections—continues to hinder their power conversion efficiency (PCE) from attaining its theoretical upper limit [34]. These defects act as recombination centers, reducing photoluminescence lifetime and causing performance losses [35–38]. Moreover, the relatively large ionic radius of the FA^+ cation presents persistent challenges to the moisture stability of FA^+ based perovskite solar cells. To address this limitation, the partial or complete substitution of FA^+ with alternative cations—either organic or inorganic—has been shown to boost both physical stability and environmental sustainability of the perovskite absorber layer, thereby contributing to the development of more durable and reliable photovoltaic devices. [18,19]. Recently Cs^+ (Cesium) is being used as a substitute of MA^+ and FA^+ cation in all-inorganic perovskite and it demonstrated superior thermal stability [39,40]. Cs^+ has a higher rate of photon absorption and could improve the PCE of PSC. According to findings by Chen et al., even though the material possesses a smaller bandgap of 1.3 eV a PCE of 12.92% was obtained in a CsSnI_3 based solar cell and in a later work Arbouz et al enhanced the efficiency of Cs^+ based PSC up to 19.92 % [41–44]. Spiro-OMeTAD was used as a HTL in many PSCs but it has its limitations. These organic HTLs are costly and volatile when exposed to moisture, elevated temperatures, and high humidity, making their cost prohibitive and limiting their life span [45]. Delafossite is a type of mineral with a crystal structure known as the delafossite structure. This structure is defined by an atomic configuration arranged in distinct layers and can be formulated as ABO_2 where A is typically univalent cation like copper (Cu^+), or silver (Ag^+), B is a trivalent cation, often a metal (M^{+3}) like Chromium (Cr^{+3}), Cobalt (Co^{+3}), Aluminium (Al^{+3}), Gallium (Fe^{+3}), Manganese (Mn^{+3}) delafossite material have a layered structure where A cations form linear chains along one axis, while the B cations are coordinated with oxygen atoms in an octahedral arrangement. This structure gives rise to unique electrical and optoelectrical properties. Delafossite materials can exhibit a range of electrical properties from being insulating to conducting. For example, copper-based delafossite like CuAlO_2 can be p-type semiconductors, which means they have holes as their majority charge carriers. Delafossite materials have good thermal and chemical stability, making them suitable to operate under high temperatures and in different environments. Among all the delafossite materials copper-based delafossite oxide have gained the most attention and have been investigated in several reports [46–48]. Delafossite CuMO_2 where $\text{M} = \text{Al, Ga, Fe, Cr, Ni, Co}$ has a hexagonal lattice structure of O-M-O and MO_6 layers [49]. TiO_2 is the most widely utilized material for the electron transport layer (ETL) among all the ETLs but it has its disadvantages. High temperature is required to fabricate TiO_2 which is very costly and TiO_2 has low electron mobility [50]. ZnO is a promising substitute of TiO_2 due to several advantageous properties. ZnO requires low fabrication temperature which reduces fabrication cost and it also offers higher electron mobility, leading to

improved performance of PSCs [50]. ZnO can be readily synthesized using the spin coating technique, which facilitates the production of smooth and uniform thin film layers [50].

Many reports previously suggested that copper-based delafossite could be a very good candidate for HTL in PSC. So, we asked the question, which copper based delafossite is the best candidate for HTL. Organic-inorganic PSCs have stability issues and perform poorly under high-temperature and humid conditions. Therefore, substituting the organic components either partially or entirely has been proposed as a viable solution for boosting stability of PSC. CsSnI₃, and CsPbI₃ are two perovskite whose organic part (FA⁺ and MA⁺) have been replaced with Cs⁺ and has better stability performance. In this work, we have used CsSnI₃ and CsPbI₃ as perovskite to create a stable solar cell. We have used Cu based delafossite CuMO₂ where M= Al, Co, Ni, Fe, Ga, and Cr to find out which delafossite is most suitable to be used as HTL. The thicknesses of both perovskite layers were systematically adjusted across the range of 100-1000 nm to determine their optimal values, while the delafossite layer thickness was altered across the range of 10-100 nm for performance optimization. Temperature of solar cells has also been varied from 300K- 350K to test the PSCs temperature tolerance and at last, we give our perspective on the performance of the simulated PSCs. This work is principally focused on creating a stable, high-performing, and economical solar cell.

2. Simulation and mathematical modeling:

The development of simulation software has opened a new era in solar cell research. Now, researchers do not have to fabricate solar cells physically and they can easily simulate different kinds of solar cell and optimize them using simulation software without any cost. Here, SCAPS is used to fabricate all the solar cells.

In SCAPS, the one-dimensional equation (1) governs the semiconductor materials under steady-state conditions. Equation 1 also illustrates the connection between the electric fields (E) of the p-n junction and the associated charge density.

$$\frac{\partial^2 \varphi}{\partial^2 x} = -\frac{\partial E}{\partial x} = \frac{\rho}{\epsilon_s} = -\frac{q}{\epsilon_s} [\rho - n + N_D^+(X) - N_A^-(X) \pm N_{\text{def}}(X)] \quad (1)$$

Here, φ represents the electrostatic potential, ϵ_s denotes the static relative permittivity of the material, and q is the charge. The terms N_D^+ , and N_A^- refer to the densities of acceptors and donors, respectively, while n and p represent the densities of electrons and holes. Equations 2 and 3 describe the carrier continuity equations within the device.

$$-\frac{\partial j_p}{\partial X} + M - V_a(a,b) = 0 - \frac{\partial j_p}{\partial X} + M - V_a(a,b) = 0 \quad (2)$$

$$-\frac{\partial j_n}{\partial X} + M - V_b(a,b) = 0 - \frac{\partial j_n}{\partial X} + M - V_b(a,b) = 0 \quad (3)$$

where, j_n = current density of electron, j_p = current density of hole, M = carrier generation, $V_b(a,b)$ = recombination of electron and $V_a(a,b)$ = hole recombination. Equations 4 and 5 represent the current density of carriers.

$$j_p = qn\mu_p E - qD_p \frac{\partial p}{\partial X} j_p = qn\mu_p E - qD_p \frac{\partial p}{\partial X} \quad (4)$$

$$j_n = qn\mu_n E - qD_n \frac{\partial n}{\partial X} j_n = qn\mu_n E - qD_n \frac{\partial n}{\partial X} \quad (5)$$

Here, q = charge, D_p , and D_n is the carrier diffusion coefficient, and μ_p and μ_n is the carrier mobilities.

3. Device configuration

This work has studied two cases (Case 1 and Case 2), and the device configuration is illustrated in Figure 1. The fundamental parameters for each layer have been sourced from relevant literature, and their values are provided in Tables 1 and 2.

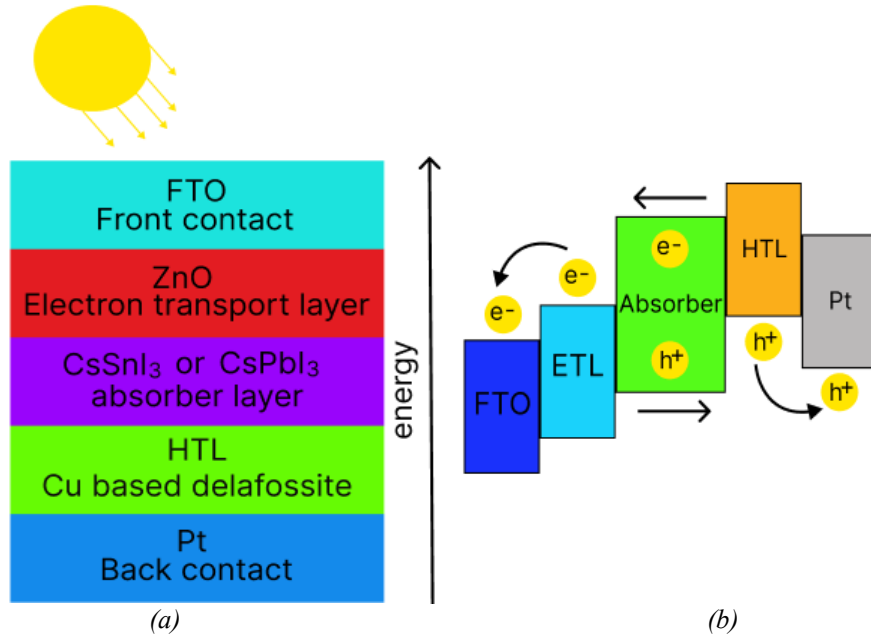


Fig. 1. Illustrates (a) the device configuration of PSC, (b) the exciton generation and carrier transport of PSC.

Table 1. The relevant values of each layer [51–59].

Parameters	FTO (TCO)	ZnO (ETL)	CsPbI ₃ (absorber layer)	CsSnI ₃ (absorber layer)
Thickness (nm)	100	10	1000	1000
E _g (eV)	3.4	3.3	1.73	1.3
χ (eV)	4.5	4.1	3.95	4.17
ε _r (eV)	9.1	9.0	6	8.2
N _c (cm ⁻³)	1.1×10 ¹⁹	2.2×10 ¹⁸	1.1×10 ²⁰	1×10 ¹⁸
N _v (cm ⁻³)	1.1×10 ¹⁹	1.9×10 ¹⁹	8×10 ¹⁹	1×10 ¹⁸
V _{th} (cm/s)	1×10 ⁷	1×10 ⁷	1×10 ⁷	1×10 ⁷
μ _n (cm ² /Vs)	20	100	16	1.6
μ _p (cm ² /Vs)	10	25	16	1.6
ND (cm ⁻³)	1.1×10 ¹⁹	1×10 ¹⁸	0	0
NA (cm ⁻³)	0	0	1×10 ¹⁵	1×10 ¹⁶

Table 2. Parameters of Cu based delafossite materials [60–77].

Parameters	CuAlO ₂	CuCoO ₂	CuNiO ₂	CuFeO ₂	CuGaO ₂	CuCrO ₂
Thickness (nm)	10	10	10	10	10	10
E _g (eV)	2.65	2.99	2.20	2.45	2.51	2.75
χ (eV)	2.43	2.30	3.30	2.65	3.10	2.99
N _c (cm ⁻³)	1 × 10 ¹⁹					
N _v (cm ⁻³)	1 × 10 ¹⁹					
μ _n (Cm ² /Vs)	11.3	0.60	1	0.64	0.20	0.15
μ _p (Cm ² /Vs)	11.3	0.60	1	0.64	0.20	0.15

4. Result and discussion

4.1. Case 1

In case 1, CsPbI₃ has been used as an absorber layer and Cu-based delafossite CuAlO₂, CuCoO₂, CuNiO₂, CuFeO₂, CuGaO₂, and CuCrO₂ has been used as HTL. ZnO has been used as ETL, FTO has been used as TCO and Pt serves as anode. Six different combinations of solar cells have been designed using six different delafossite materials. All the solar cells have been optimized by varying the perovskite layer thickness, HTL thickness, and temperature to see which delafossite material performs best.

4.1.1. Thickness

The influence of CsPbI₃ absorber layers thickness on FF, Voc, Jsc, and PCE was tested through thickness variation of CsPbI₃, ranging from 100-1000 nm, while all the other parameters were fixed. With the increase in thickness, the values of Voc of all six PSCs started to increase. The highest value of Voc of all PSCs was recorded at 1000 nm thickness. At 1000 nm thickness the Voc of CuAlO₂, CuCoO₂, CuNiO₂, CuFeO₂, CuGaO₂, and CuCrO₂ based PSCs were 0.8518 V, 1.0290 V, 1.1710 V, 0.8717 V, 1.1816 V, 1.2281 V respectively. The value of Jsc started to increase with increasing thickness and the highest values of Jsc were recorded at 1000 nm thickness for all PSCs. The recorded values of CuAlO₂, CuCoO₂, CuNiO₂, CuFeO₂, CuGaO₂, and CuCrO₂ based solar cells at 1000 nm thickness were 20.457682 mA/Cm², 20.481282 mA/Cm², 20.486112 mA/Cm², 20.462464 mA/Cm², 20.485819 mA/Cm², and 20.485776 mA/Cm², respectively. PCE of all PSCs was also observed to increase with increasing thickness of perovskite. All the PSCs exhibited the maximum PCE at a thickness of 1000 nm. The highest recorded PCE of CuAlO₂, CuCoO₂, CuNiO₂, CuFeO₂, CuGaO₂, and CuCrO₂ based PSCs at 1000 nm thickness were 13.79 %, 17.64 %, 20.81 %, 14.15 %, 20.87 %, and 20.90 % respectively. As the thickness of the CsPbI₃ was increasing a continuous drop in FF was observed. At 1000 nm thickness the values of FF of CuAlO₂, CuCoO₂, CuNiO₂, CuFeO₂, CuGaO₂, and CuCrO₂ based PSCs were 79.12 %, 83.72 %, 86.75 %, 79.34 %, 86.21 %, and 86.20 % respectively. The highest FF of all PSCs was recorded at 100 nm perovskite thickness and the generation of a strong electric field across the absorber layer were responsible for this high FF. As the thickness increased this electric field decreased and a quasi-neutral state was created within the absorber layer, this quasi-neutral region means electrons move via diffusion which causes series resistance to rise and as a result FF drops [78,79]. The increase in Voc with greater thickness suggests that recombination within the quasi-neutral region is not the predominant mechanism, preventing a significant increase in reverse saturation current [78,80]. The persistent rise in Jsc can be attributed to the high absorption coefficient of the perovskite material [81]. With the increase in CsPbI₃ thickness PCE increases because of high absorption in a bulk absorber layer [80,81].

4.1.2. HTL Thickness

The thickness of the HTL was adjusted within the range of 10-100 nm to investigate its influence on the performance of the PSC. As the thickness increased, all the values of all parameters almost became saturated at 20 nm. So, the values of all PSCs were kept at 10 nm. At 10 nm the highest recorded PCE of CuAlO₂, CuCoO₂, CuNiO₂, CuFeO₂, CuGaO₂, and CuCrO₂ based PSCs were 15.35 %, 16.50 %, 18.58 %, 15.63 %, 19.48 %, 19.52 %.

4.1.3. Temperature

The solar cell gets heated by the sun continuously during day time and this temperature rise can have some adverse on solar cells performance. To investigate the impression of temperature on PSC the temperature was varied from 300K to 350K. As the temperature rises Voc, FF, and PCE of all the six PSCs started to drop but a corresponding rise in Jsc was observed. Voc decreased when the temperature climbed because the reverse saturation current increased as well [82]. An increase in Jsc results from the absorber layer's bandgap narrowing with temperature, which permits more charge carriers to move from the valence band to the conduction band [82]. The rise in Jsc was not very significant in influencing the performance of PSC. Due to their dependency on Voc and Jsc both FF and PCE drops with increasing temperature. The highest-recorded PCE of CuAlO₂, CuCoO₂, CuNiO₂, CuFeO₂, CuGaO₂, and CuCrO₂ based PSCs at 300K were 13.79 %, 17.64 %, 20.81 %, 14.15 %, 20.87 %, and 20.90 % respectively.

4.1.4. Observation

In case 1, it was observed that the peak value of Jsc, PCE and Voc was recorded at 1000 nm perovskite thickness, 10 nm HTL thickness, and 300 k temperature. However, the highest FF value was observed with a perovskite thickness of 100 nm. Among all the PSCs designed CuNiO₂ based PSC have shown the highest value of Jsc, and FF, and the optimal value of Voc, and PCE was shown by CuCrO₂ based PSC. One of the most desirable qualities of PSC is its PCE. Solar cells can produce high-output power if it has high PCE and it is evident from case 1 that CuCrO₂ based PSC has performed the best in terms of PCE.

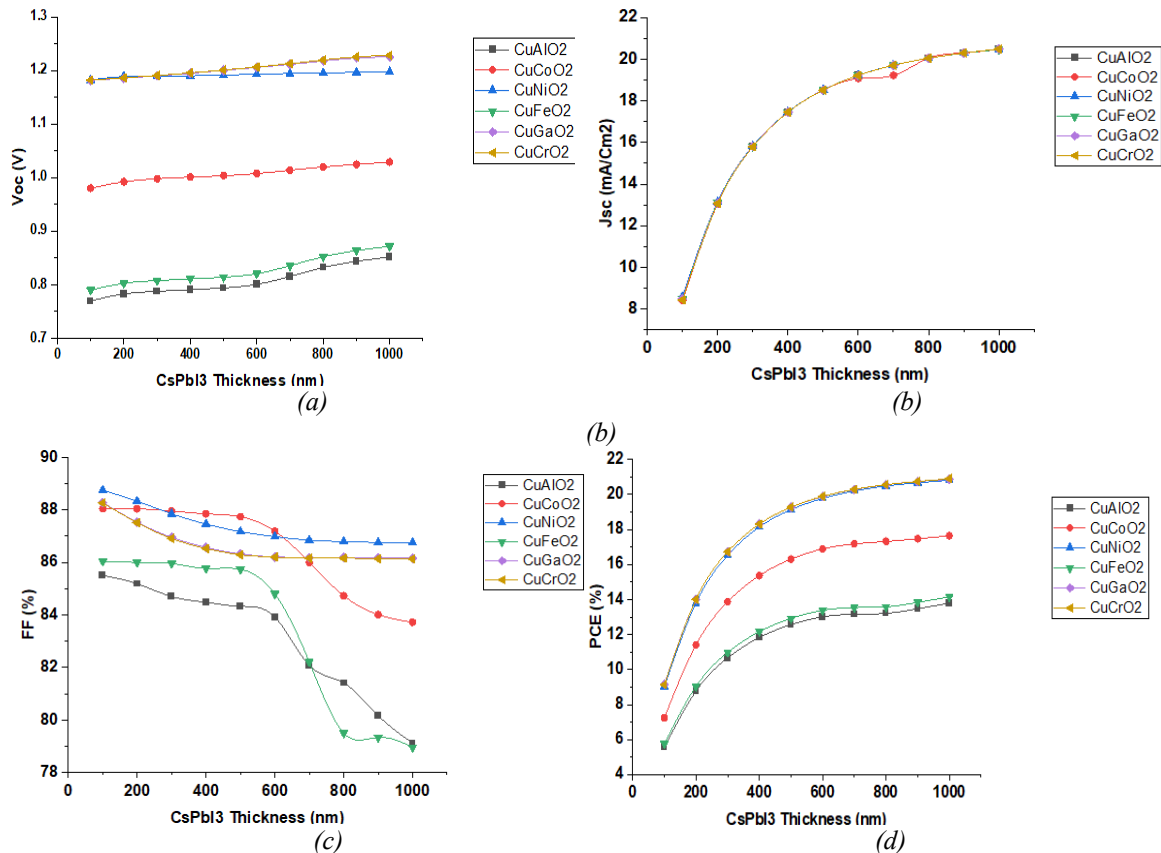


Fig. 2. Illustrates the impact of perovskite thickness on (a) Voc, (b) Jsc, (c) FF, and (d) PCE of all PSCs of case 1.

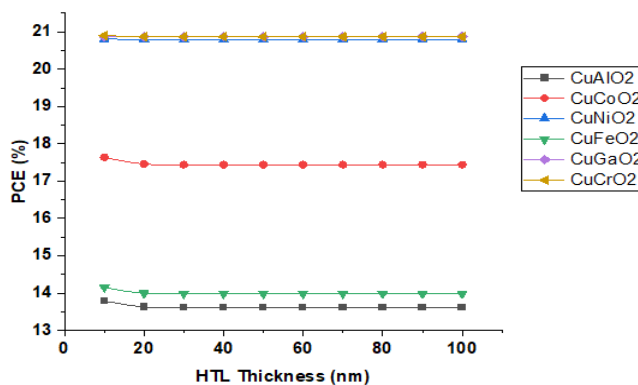


Fig. 3. Demonstrates the effect of HTL thickness on PCE of case 1.

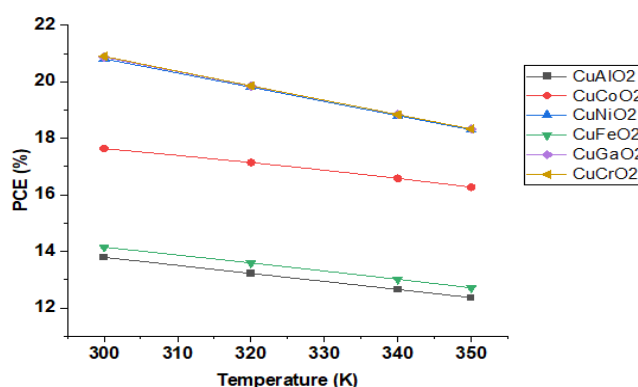


Fig. 4. Demonstrates how temperature affects the PCE of case 1.

4.2. Case 2

In case 2, CsSnI_3 have been used as absorber layer and Cu-based delafossite CuAlO_2 , CuCoO_2 , CuNiO_2 , CuFeO_2 , CuGaO_2 , and CuCrO_2 has been used as HTL. ZnO has been used as ETL and FTO has been used as TCO and Pt has been used as anode. Like case 1, six different solar cells have been created using six different delafossite materials and the effect of perovskite thickness, HTL thickness, and temperature has been tested.

4.2.1. Perovskite thickness

Keeping all other device parameters constant, the CsSnI_3 thickness was varied from 100 nm to 1000 nm in order to systematically investigate the impact of perovskite layer thickness on device performance. The impact of absorber layer thickness on overall solar cell performance was assessed by analyzing the consequent effects on FF, V_{oc} , PCE, and J_{sc} . With increasing thickness, the value of V_{oc} started to increase and the highest V_{oc} of all six PSCs were recorded at 1000 nm thickness. At 1000 nm thickness the value of V_{oc} of CuAlO_2 , CuCoO_2 , CuNiO_2 , CuFeO_2 , CuGaO_2 , and CuCrO_2 based PSCs were 0.4038 V, 0.5871 V, 0.7772 V, 0.4133 V, 0.8587 V, and 0.9451 V respectively. J_{sc} also started to increase with thickness and at 1000 nm thickness the highest value of J_{sc} of all PSCs was recorded. The values of J_{sc} of CuAlO_2 , CuCoO_2 , CuNiO_2 , CuFeO_2 , CuGaO_2 , and CuCrO_2 based PSCs were $30.513076 \text{ mA}/\text{cm}^2$, $35.525720 \text{ mA}/\text{cm}^2$, $35.536710 \text{ mA}/\text{cm}^2$, $35.507494 \text{ mA}/\text{cm}^2$, $35.538561 \text{ mA}/\text{cm}^2$, and $35.539482 \text{ mA}/\text{cm}^2$ respectively. PCE was also observed to increase with increasing thickness of perovskite and the highest PCE of CuAlO_2 , CuCoO_2 , CuNiO_2 , CuFeO_2 , and CuGaO_2 based PSCs were 10.43 %, 16.12 %, 22.87 %, 10.68 %, and 25.68 % respectively at 1000 nm thickness. Unlike other PSCs the highest value of PCE of CuCrO_2 based PSC was recorded at 900 nm thickness and the PCE was 26.34 %.

4.2.2. HTL thickness

By modifying the HTL thickness from 10 nm to 100 nm, the effect of HTL thickness on PSC performance was examined. The analysis revealed that changes in HTL thickness within this range did not produce any significant variation in device performance. No noticeable change in PSC performance was noted as the thickness of HTL increased from 10 nm, and the values of FF, Voc, PCE, and Jsc almost became saturated at 20 nm thickness. The peak values of all PSCs were recorded at 10 nm thickness and the PCE of CuAlO₂, CuCoO₂, CuNiO₂, CuFeO₂, CuGaO₂, and CuCrO₂ based PSCs were 10.43 %, 16.12 %, 22.87 %, 10.68 %, 25.68 %, and 26.34 % respectively.

4.2.3. Temperature

The effect of temperature on case 2 was similar to case 1. The performance of all solar cells started to deteriorate gradually with increasing temperature. Voc, FF, and PCE started to deteriorate as the temperature started to rise above 300 K but like case 1, a slight rise in Jsc was observed. The highest value of PCE of CuAlO₂, CuCoO₂, CuNiO₂, CuFeO₂, CuGaO₂, and CuCrO₂ based PSCs at 300K temperature were 10.43 %, 16.12 %, 22.87 %, 10.68 %, 25.68 %, and 26.34 % respectively.

4.2.4. Observation

In case 2, the highest value of Voc, and Jsc of all PSCs were recorded at 1000 nm Perovskite thickness, 10 nm of HTL thickness, and 300 K temperature. The highest value of five PSCs (except CuCrO₂ based PSC) were recorded at the same parameters but the highest PCE of CuCrO₂ based PSC was recorded at 900 nm perovskite thickness which is the highest among all PSCs.

In both cases, the highest PCE was produced by CuCrO₂ based PSCs. So, it can be said that CuCrO₂ based PSCs have performed the best among all simulated devices.

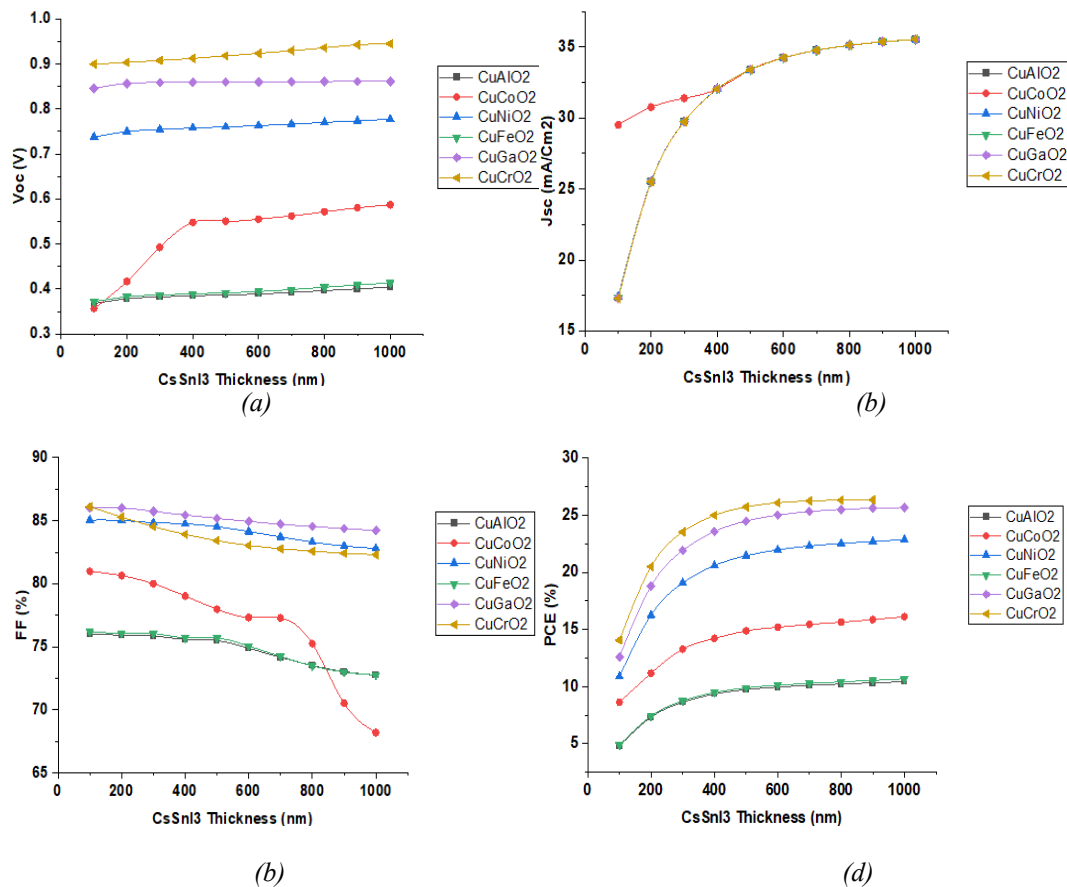


Fig. 5. Illustrates the impact of perovskite thickness on (a) Voc, (b) Jsc, (c) FF, and (d) PCE of all PSCs of case 2.

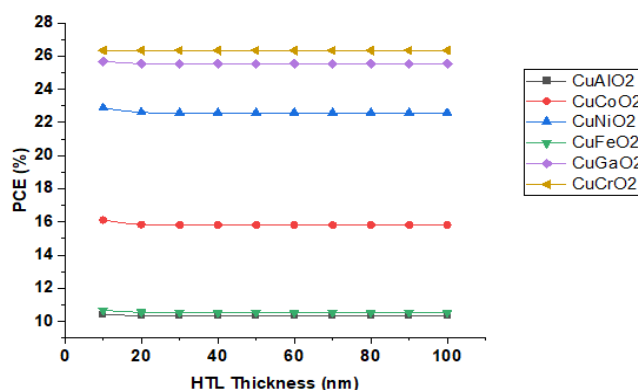


Fig. 6. Demonstrates the effect of HTL thickness on PCE of case 2.

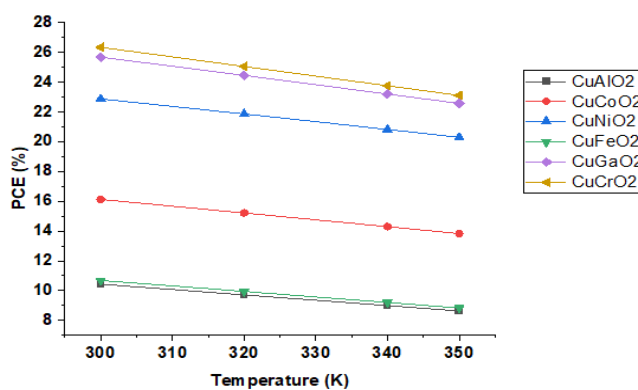


Fig. 7. Demonstrates how temperature affects the PCE of case 2.

5. Conclusion

In this study, in case 1, all the PSCs showed highest V_{oc} , J_{sc} , and PCE at 1000 nm perovskite thickness, 10 nm HTL thickness, and 300K temperature. Out of all the other PSCs $CuCrO_2$ based solar cell has demonstrated the highest PCE, J_{sc} , and V_{oc} . However, the highest values of FF were recorded at 100 nm thickness. It is evident from the study that elevated temperatures exhibited a detrimental influence on the performance of PSCs. The PCE of all the PSCs started to decline gradually with increasing temperature. In case 2, all the PSCs have shown the highest value of V_{oc} , and J_{sc} at 1000 nm perovskite thickness, 10 nm HTL thickness, and 300 K temperature. The highest PCE of all solar cells except $CuCrO_2$ based PSC were recorded at 1000 nm of perovskite thickness and the highest value of $CuCrO_2$ based solar cell was recorded at 900 nm perovskite thickness. The highest FF of all PSCs was obtained at 100 nm perovskite thickness.

6. Future work

Solar cell has a lot of potential not only in energy sector but also in sectors like healthcare and biomedical engineering. As the world is moving towards self-powered healthcare devices, solar cell can be a great replacement of batteries. Many healthcare devices use piezo material for energy harvesting which has a low energy output [83-87]. Solar cell can be used as an additional energy source on those devices to solve the energy issue.

Declaration of competing interest

The authors confirm they have no conflict of interest to disclose regarding this manuscript. None of the authors have financial associations, professional relationships, or personal connections that might bias the results or conclusions reported herein.

Acknowledgments

The authors thank East Delta University for its sincere help in this work. Special appreciation is extended to the supervisor for invaluable assistance and unwavering encouragement throughout the work. His expertise and insights significantly contributed to the quality and depth of this work.

References

- [1] S. Sahota, G. Shah, P. Ghosh, R. Kapoor, S. Sengupta, P. Singh, V. Vijay, A. Sahay, V.K. Vijay, I.S. Thakur, *Bioresour Technol Rep* 1 (2018) 79-88; <https://doi.org/10.1016/j.biteb.2018.01.002>
- [2] C. Gürsan, V. de Gooyert, *Renewable and Sustainable Energy Reviews* 138 (2021) 110552; <https://doi.org/10.1016/j.rser.2020.110552>
- [3] Y.S. Mohammed, A.S. Mokhtar, N. Bashir, R. Saidur, *Renewable and Sustainable Energy Reviews* 20 (2013) 15-25; <https://doi.org/10.1016/j.rser.2012.11.047>
- [4] M. Al-Ali, I. Dincer, *Appl Therm Eng* 71 (2014) 16-23; <https://doi.org/10.1016/j.applthermaleng.2014.06.033>
- [5] R.P. Singh, H.P. Nachtnebel, *Renewable and Sustainable Energy Reviews* 55 (2016) 43-58; <https://doi.org/10.1016/j.rser.2015.10.138>
- [6] A. Bahrami, C.O. Okoye, U. Atikol, *Renew Energy* 113 (2017) 563-579; <https://doi.org/10.1016/j.renene.2017.05.095>
- [7] A. Bahrami, C.O. Okoye, *Renewable and Sustainable Energy Reviews* 97 (2018) 138-151; <https://doi.org/10.1016/j.rser.2018.08.035>
- [8] C.O. Okoye, A. Bahrami, U. Atikol, *Renewable and Sustainable Energy Reviews* 81 (2018) 1569-1581; <https://doi.org/10.1016/j.rser.2017.05.235>
- [9] A. Bahrami, A. Teimourian, C.O. Okoye, H. Shiri, *J Clean Prod* 223 (2019) 801-814; <https://doi.org/10.1016/j.jclepro.2019.03.140>
- [10] A. Teimourian, A. Bahrami, H. Teimourian, M. Vala, A. Oraj Huseyniklioglu, *Energy Sources, Part A: Recovery, Utilization, and Environmental Effects* 42 (2020) 329-343; <https://doi.org/10.1080/15567036.2019.1587079>
- [11] Renewable capacity statistics 2023., 2023.
- [12] M. Wang, W. Wang, B. Ma, W. Shen, L. Liu, K. Cao, S. Chen, W. Huang, *Nanomicro Lett* 13 (2021) 62; <https://doi.org/10.1007/s40820-020-00578-z>
- [13] V. D'Innocenzo, G. Grancini, M.J.P. Alcocer, A.R.S. Kandada, S.D. Stranks, M.M. Lee, G. Lanzani, H.J. Snaith, A. Petrozza, *Nat Commun* 5 (2014) 3586; <https://doi.org/10.1038/ncomms4586>
- [14] S.D. Stranks, G.E. Eperon, G. Grancini, C. Menelaou, M.J.P. Alcocer, T. Leijtens, L.M. Herz, A. Petrozza, H.J. Snaith, *Science* (1979) 342 (2013) 341-344; <https://doi.org/10.1126/science.1243982>
- [15] J.S. Manser, P. V. Kamat, *Nat Photonics* 8 (2014) 737-743; <https://doi.org/10.1038/nphoton.2014.171>

- [16] T. Baikie, Y. Fang, J.M. Kadro, M. Schreyer, F. Wei, S.G. Mhaisalkar, M. Graetzel, T.J. White, *J Mater Chem A Mater* 1 (2013) 5628; <https://doi.org/10.1039/c3ta10518k>
- [17] Al.A. Siddique, S. Bin Helal, M.I. Haque, *Journal of Ovonic Research* 20 (2024) 187-200; <https://doi.org/10.15251/JOR.2024.202.187>
- [18] M. Saliba, T. Matsui, K. Domanski, J.-Y. Seo, A. Ummadisingu, S.M. Zakeeruddin, J.-P. Correa-Baena, W.R. Tress, A. Abate, A. Hagfeldt, M. Grätzel, *Science* (1979) 354 (2016) 206-209; <https://doi.org/10.1126/science.aah5557>
- [19] J. Lee, D. Kim, H. Kim, S. Seo, S.M. Cho, N. Park, *Adv Energy Mater* 5 (2015); <https://doi.org/10.1002/aenm.201501310>
- [20] B. Conings, J. Drijkoningen, N. Gauquelin, A. Babayigit, J. D'Haen, L. D'Olieslaeger, A. Ethirajan, J. Verbeeck, J. Manca, E. Mosconi, F. De Angelis, H. Boyen, *Adv Energy Mater* 5 (2015); <https://doi.org/10.1002/aenm.201500477>
- [21] T.A. Berhe, W.-N. Su, C.-H. Chen, C.-J. Pan, J.-H. Cheng, H.-M. Chen, M.-C. Tsai, L.-Y. Chen, A.A. Dubale, B.-J. Hwang, *Energy Environ Sci* 9 (2016) 323-356; <https://doi.org/10.1039/C5EE02733K>
- [22] C.C. Stoumpos, C.D. Malliakas, M.G. Kanatzidis, *Inorg Chem* 52 (2013) 9019-9038; <https://doi.org/10.1021/ic401215x>
- [23] Y. Han, S. Meyer, Y. Dkhissi, K. Weber, J.M. Pringle, U. Bach, L. Spiccia, Y.-B. Cheng, *J Mater Chem A Mater* 3 (2015) 8139-8147; <https://doi.org/10.1039/C5TA00358J>
- [24] R.K. Misra, S. Aharon, B. Li, D. Mogilyansky, I. Visoly-Fisher, L. Etgar, E.A. Katz, *J Phys Chem Lett* 6 (2015) 326-330; <https://doi.org/10.1021/jz502642b>
- [25] X. Liu, Y. Zhang, J. Hua, Y. Peng, F. Huang, J. Zhong, W. Li, Z. Ku, Y. Cheng, *RSC Adv* 8 (2018) 14991-14994; <https://doi.org/10.1039/C7RA13611K>
- [26] T.M. Koh, K. Fu, Y. Fang, S. Chen, T.C. Sum, N. Mathews, S.G. Mhaisalkar, P.P. Boix, T. Baikie, *The Journal of Physical Chemistry C* 118 (2014) 16458-16462; <https://doi.org/10.1021/jp411112k>
- [27] G.E. Eperon, S.D. Stranks, C. Menelaou, M.B. Johnston, L.M. Herz, H.J. Snaith, *Energy Environ Sci* 7 (2014) 982; <https://doi.org/10.1039/c3ee43822h>
- [28] S. Pang, H. Hu, J. Zhang, S. Lv, Y. Yu, F. Wei, T. Qin, H. Xu, Z. Liu, G. Cui, *Chemistry of Materials* 26 (2014) 1485-1491; <https://doi.org/10.1021/cm404006p>
- [29] N. Pellet, P. Gao, G. Gregori, T. Yang, M.K. Nazeeruddin, J. Maier, M. Grätzel, *Angewandte Chemie International Edition* 53 (2014) 3151-3157; <https://doi.org/10.1002/anie.201309361>
- [30] J. Lee, D. Seol, A. Cho, N. Park, *Advanced Materials* 26 (2014) 4991-4998; <https://doi.org/10.1002/adma.201401137>
- [31] M. Hu, L. Liu, A. Mei, Y. Yang, T. Liu, H. Han, *J. Mater. Chem. A* 2 (2014) 17115-17121; <https://doi.org/10.1039/C4TA03741C>
- [32] A. Binek, F.C. Hanusch, P. Docampo, T. Bein, *J Phys Chem Lett* 6 (2015) 1249-1253; <https://doi.org/10.1021/acs.jpcclett.5b00380>
- [33] J.-W. Lee, S.H. Lee, H.-S. Ko, J. Kwon, J.H. Park, S.M. Kang, N. Ahn, M. Choi, J.K. Kim, N.-G. Park, *J Mater Chem A Mater* 3 (2015) 9179-9186; <https://doi.org/10.1039/C4TA04988H>
- [34] Y. Zhang, S.-G. Kim, D. Lee, H. Shin, N.-G. Park, *Energy Environ Sci* 12 (2019) 308-321; <https://doi.org/10.1039/C8EE02730G>
- [35] Q. Jiang, Y. Zhao, X. Zhang, X. Yang, Y. Chen, Z. Chu, Q. Ye, X. Li, Z. Yin, J. You, *Nat Photonics* 13 (2019) 460-466; <https://doi.org/10.1038/s41566-019-0398-2>
- [36] National Renewable Energy Laboratory Best Research-Cell Efficiency Chart., 2024.
- [37] J.J. Yoo, G. Seo, M.R. Chua, T.G. Park, Y. Lu, F. Rotermund, Y.-K. Kim, C.S. Moon, N.J. Jeon, J.-P. Correa-Baena, V. Bulović, S.S. Shin, M.G. Bawendi, J. Seo, *Nature* 590 (2021) 587-593; <https://doi.org/10.1038/s41586-021-03285-w>
- [38] H.J. Snaith, *Nat Mater* 17 (2018) 372-376; <https://doi.org/10.1038/s41563-018-0071-z>

- [39] Y. Wang, M.I. Dar, L.K. Ono, T. Zhang, M. Kan, Y. Li, L. Zhang, X. Wang, Y. Yang, X. Gao, Y. Qi, M. Grätzel, Y. Zhao, *Science* (1979) 365 (2019) 591-595; <https://doi.org/10.1126/science.aav8680>
- [40] H. Wang, H. Bian, Z. Jin, H. Zhang, L. Liang, J. Wen, Q. Wang, L. Ding, S.F. Liu, *Chemistry of Materials* 31 (2019) 6231-6238; <https://doi.org/10.1021/acs.chemmater.9b02248>
- [41] L.-J. Chen, C.-R. Lee, Y.-J. Chuang, Z.-H. Wu, C. Chen, *J Phys Chem Lett* 7 (2016) 5028-5035; <https://doi.org/10.1021/acs.jpcclett.6b02344>
- [42] K. Shum, Z. Chen, J. Qureshi, C. Yu, J.J. Wang, W. Pfenninger, N. Vockic, J. Midgley, J.T. Kenney, *Appl Phys Lett* 96 (2010); <https://doi.org/10.1063/1.3442511>
- [43] Z. Chen, C. Yu, K. Shum, J.J. Wang, W. Pfenninger, N. Vockic, J. Midgley, J.T. Kenney, *J Lumin* 132 (2012) 345-349; <https://doi.org/10.1016/j.jlumin.2011.09.006>
- [44] H. Arbouz, *Applied Rheology* 33 (2023); <https://doi.org/10.1515/arh-2022-0138>
- [45] S. Yun, Y. Qin, A.R. Uhl, N. Vlachopoulos, M. Yin, D. Li, X. Han, A. Hagfeldt, *Energy Environ Sci* 11 (2018) 476-526; <https://doi.org/10.1039/C7EE03165C>
- [46] C. Baiano, E. Schiavo, C. Gerbaldi, F. Bella, G. Meligrana, G. Talarico, P. Maddalena, M. Pavone, A.B. Muñoz-García, *Molecular Catalysis* 496 (2020) 111181; <https://doi.org/10.1016/j.mcat.2020.111181>
- [47] J. Pellicer-Porres, A. Segura, D. Kim, *Semicond Sci Technol* 24 (2009) 015002; <https://doi.org/10.1088/0268-1242/24/1/015002>
- [48] N. Sahu, B. Parija, S. Panigrahi, *Indian Journal of Physics* 83 (2009) 493-502; <https://doi.org/10.1007/s12648-009-0009-z>
- [49] R.A. Afre, N. Sharma, M. Sharon, M. Sharon, *Reviews on Advanced Materials Science* 53 (2018) 79-89; <https://doi.org/10.1515/rams-2018-0006>
- [50] M. Dehghan, A. Behjat, *RSC Adv* 9 (2019) 20917-20924; <https://doi.org/10.1039/C9RA01839E>
- [51] P.K. Patel, *Sci Rep* 11 (2021) 3082; <https://doi.org/10.1038/s41598-021-82817-w>
- [52] S. Ahmed, F. Jannat, Md.A.K. Khan, M.A. Alim, *Optik* 225 (2021) 165765; <https://doi.org/10.1016/j.ijleo.2020.165765>
- [53] F. Baig, *Universitat Politècnica de València*, 2019; <https://doi.org/10.4995/Thesis/10251/118801>
- [54] I. Kabir, S.A. Mahmood, *IEEE*, 2019: pp. 1-4; <https://doi.org/10.1109/ICTP48844.2019.9041784>
- [55] Gagandeep, M. Singh, R. Kumar, Simulation of perovskite solar cell with graphene as hole transporting material, in: 2019: p. 030548; <https://doi.org/10.1063/1.5113387>
- [56] M.A. Rahman, *Opt Mater Express* 12 (2022) 2954; <https://doi.org/10.1364/OME.465498>
- [57] C. Devi, R. Mehra, *J Mater Sci* 54 (2019) 5615-5624; <https://doi.org/10.1007/s10853-018-03265-y>
- [58] S. Bhattarai, M.K. Hossain, R. Pandey, J. Madan, D.P. Samajdar, M. Chowdhury, Md.F. Rahman, M.Z. Ansari, M.D. Albaqami, *Heliyon* 10 (2024) e24107; <https://doi.org/10.1016/j.heliyon.2024.e24107>
- [59] U. ur Rehman, R.S. Almufarij, K. ul Sahar, E.A. Shokralla, A. Ashfaq, K. Mahmood, E. Hussain, H.A. Alsalmah, R.Y. Capangpangan, A.C. Alguno, *Optik* 293 (2023) 171392; <https://doi.org/10.1016/j.ijleo.2023.171392>
- [60] H. Chfii, A. Bouich, B.M. Soucase, M. Abdlefdil, *Opt Mater (Amst)* 135 (2023) 113229; <https://doi.org/10.1016/j.optmat.2022.113229>
- [61] R. Chouhan, A. Agrawal, M. Gupta, P. Sen, *Physica Status Solidi (b)* 259 (2022); <https://doi.org/10.1002/pssb.202100132>
- [62] S. Haque, M. Alexandre, M.J. Mendes, H. Águas, E. Fortunato, R. Martins, *Appl Mater Today* 20 (2020) 100720; <https://doi.org/10.1016/j.apmt.2020.100720>

- [63] L. Li, Y. Wu, E. Li, C. Shen, H. Zhang, X. Xu, G. Wu, M. Cai, W.-H. Zhu, *Chemical Communications* 55 (2019) 13239-13242; <https://doi.org/10.1039/C9CC06345E>
- [64] X. Liu, J. Chen, M. Luo, M. Leng, Z. Xia, Y. Zhou, S. Qin, D.-J. Xue, L. Lv, H. Huang, D. Niu, J. Tang, *ACS Appl Mater Interfaces* 6 (2014) 10687-10695; <https://doi.org/10.1021/am502427s>
- [65] M. Moreira, J. Afonso, J. Crepelliere, D. Lenoble, P. Lunca-Popa, *J Mater Sci* 57 (2022) 3114-3142; <https://doi.org/10.1007/s10853-021-06815-z>
- [66] R. K. H. Reddy, U. S, *Frontiers in Nanoscience and Nanotechnology* 3 (2017); <https://doi.org/10.15761/FNN.1000154>
- [67] C. Ruttanapun, M. Sa-nguan-cheep, S. Kahatta, P. Buranasiri, P. Jindajitawat, Optical and electronic transport properties of p -type CuCoO 2 transparent conductive oxide, in: P. Buranasiri, S. Sumriddetchkajorn (Eds.), 2013: p. 888310; <https://doi.org/10.1117/12.2021992>
- [68] T.S. Tripathi, J.-P. Niemelä, M. Karppinen, *J Mater Chem C Mater* 3 (2015) 8364-8371; <https://doi.org/10.1039/C5TC01384D>
- [69] I. Sinnarasa, Y. Thimont, L. Presmanes, A. Barnabé, P. Tailhades, *Nanomaterials* 7 (2017) 157; <https://doi.org/10.3390/nano7070157>
- [70] A. Sreedhar, M. Hari Prasad Reddy, S. Uthanna, J.F. Pierson, *ISRN Condensed Matter Physics* 2013 (2013) 1-9; <https://doi.org/10.1155/2013/527341>
- [71] H. Zhang, H. Wang, W. Chen, A.K. -Y. Jen, *Advanced Materials* 29 (2017); <https://doi.org/10.1002/adma.201604984>
- [72] Z.Q. Yao, B. He, L. Zhang, C.Q. Zhuang, T.W. Ng, S.L. Liu, M. Vogel, A. Kumar, W.J. Zhang, C.S. Lee, S.T. Lee, X. Jiang, *Appl Phys Lett* 100 (2012); <https://doi.org/10.1063/1.3683499>
- [73] H. Bouakaz, M. Abbas, R. Brahim, M. Trari, *Mater Sci Semicond Process* 136 (2021) 106132; <https://doi.org/10.1016/j.mssp.2021.106132>
- [74] A.N.A.M. Sayedmohsen Shahshahan, *Increased Open Circuit Voltage Using Copper-Based Oxide Semiconductors as Photocathodes in p-Type Dye-Sensitized Solar Cells*, University of Wollongong, 2020.
- [75] S. Akin, F. Sadegh, S. Turan, S. Sonmezoglu, *ACS Appl Mater Interfaces* 11 (2019) 45142-45149; <https://doi.org/10.1021/acsami.9b14740>
- [76] M.-S. Miao, S. Yarbro, P.T. Barton, R. Seshadri, *Phys Rev B* 89 (2014) 045306; <https://doi.org/10.1103/PhysRevB.89.045306>
- [77] N. Benreguia, A. Abdi, O. Mahroua, M. Trari, *Journal of Solid State Electrochemistry* 22 (2018) 2499-2506; <https://doi.org/10.1007/s10008-018-3967-2>
- [78] Y. Takahashi, H. Hasegawa, Y. Takahashi, T. Inabe, *J Solid State Chem* 205 (2013) 39-43; <https://doi.org/10.1016/j.jssc.2013.07.008>
- [79] H.-J. Du, W.-C. Wang, J.-Z. Zhu, *Chinese Physics B* 25 (2016) 108802; <https://doi.org/10.1088/1674-1056/25/10/108802>
- [80] F. Hao, C.C. Stoumpos, D.H. Cao, R.P.H. Chang, M.G. Kanatzidis, *Nat Photonics* 8 (2014) 489-494; <https://doi.org/10.1038/nphoton.2014.82>
- [81] L. Ma, F. Hao, C.C. Stoumpos, B.T. Phelan, M.R. Wasielewski, M.G. Kanatzidis, *J Am Chem Soc* 138 (2016) 14750-14755; <https://doi.org/10.1021/jacs.6b09257>
- [82] P. Roy, N. Kumar Sinha, A. Khare, *Mater Today Proc* 39 (2021) 2022-2026; <https://doi.org/10.1016/j.matpr.2020.09.281>
- [83] M. I. Haque, K. Yoshibayashi, J. Wang, G. Fischer, J. Kirchner, "Design and Evaluation of Directional Antenna for Shoe-mounted Sensor for Position Identification of Elderly Wanderer", *Sensing and Bio- Sensing Research*, Elsevier, Volume 34, December 2021, 100451 ([doi: 10.1016/j.sbsr.2021.100451](https://doi.org/10.1016/j.sbsr.2021.100451)).
- [84] M. I. Haque, K. Yoshibayashi, J. Wang, G. Fischer and J. Kirchner, "Directive Antenna Design at 2.4 GHz on Foot Surface for Wanderer Location Identification," 2020 International

Symposium on Antennas and Propagation (ISAP), 2021, pp. 635-636, ([doi: 10.23919/ISAP47053.2021.9391396](https://doi.org/10.23919/ISAP47053.2021.9391396)).

[85] M. I. Haque, R. Yamada, J. Shi, J. Wang, D. Anzai, "Channel Characteristics and Link Budget Analysis for 10-60 MHz Band Implant Communication", IEICE Transactions on Communications, Apr. 2021, Vol. E 104-B, No.4,410-418 ([DOI: 10.1587/transcom.2020EBP3075](https://doi.org/10.1587/transcom.2020EBP3075)).

[86] M. I. Haque, R. Yamamoto, J. Wang and K. -I. Kakimoto, "Measurement Performance of NKN Piezo Material for Powering Shoe-mounted Sensor," 2022 International Conference on Innovations in Science, Engineering and Technology (ICISSET), 2022, pp. 324-328, ([doi: 10.1109/ICISSET54810.2022.9775861](https://doi.org/10.1109/ICISSET54810.2022.9775861)).

[87] M. I. Haque, J. Wang, D. Anzai, "Path Loss and Group Delay Analysis at 10-60 MHz Human Body Communication Band", IEICE Technical Report, EMCJ2019-78,13th Dec 2019,19-22.